DOI: 10.1002/chem.200800632

# A Mesoporous 3D Hybrid Material with Dual Functionality for $Hg^{2+}$ Detection and Adsorption

José V. Ros-Lis,[a] Rosa Casasús,[a] María Comes,[a] Carmen Coll,[a] M. Dolores Marcos,[a] Ramón Martínez-Máñez,*[a] Félix Sancenón,[a] Juan Soto,[a] Pedro Amorós,*[b] Jamal El Haskouri,[b] Nuria Garró,[b] and Knut Rurack*[c]

**Abstract:** Dual-function hybrid material **U1** was designed for simultaneous chromofluorogenic detection and removal of $Hg^{2+}$ in an aqueous environment. Mesoporous material **UVM-7** (MCM41 type) with homogeneously distributed pores of about 2–3 nm in size, a large specific surface area exceeding 1000 $m^2 g^{-1}$, and nanoscale particles was used as an inorganic support. The mesoporous solid is decorated with thiol groups that were treated with squaraine dye **III** to give a 2,4-bis(4-dialkylaminophenyl)-3-hydroxy-4-alkylsulfanylcyclobut-2-enone (APC) derivative that is covalently anchored to the inorganic silica matrix. The solid was characterised by various techniques including X-ray diffraction, transmission electron microscopy, Raman spectroscopy, and nitrogen adsorption. This hybrid solid is the chemodosimeter for $Hg^{2+}$ detection. $Hg^{2+}$ reacts with the APC fragment in **U1** with release of the squaraine dye into the solution, which turns deep blue and fluoresces strongly. Naked-eye $Hg^{2+}$ detection is thus accomplished in an easy-to-use procedure. In contrast, **U1** remains silent in the presence of other thiophilic transition metal ions, alkali and alkaline earth metal ions, or anions ubiquitously present in water such as chloride, carbonate, sulfate, and phosphate. Material **U1** acts not only as chemodosimeter that signals the presence of $Hg^{2+}$ down to parts-per-billion concentrations, but at the same time is also an excellent adsorbent for the removal of mercury cations from aqueous solutions. The amount of adsorbed mercury ranges from 0.7 to 1.7 mmol $g^{-1}$, depending on the degree of functionalisation. In addition, hybrid material **U1** can be regenerated for both sensing and removal purposes. As far as we know, **U1** is the first example of a promising new class of polyfunctional hybrid supports that can be used as both remediation and alarm systems by selective signalling and removal of target species of environmental importance. Model compounds based on silica gel (**G1**), fumed silica (**F1**), and micrometre-sized MCM-41 scaffolds (**M1**) were also prepared and studied for comparative purposes.

**Keywords:** dyes/pigments · environmental chemistry · mercury · mesoporous materials · sensors

## Introduction

Although pre-industrial manufacturing liberated considerable amounts of toxic heavy metals into the environment,[1] the industrial revolution in particular not only raised the prosperity of mankind, but significantly increased pollution of the anthroposphere and natural habitats with heavy metals.[2] One of the most important heavy metal contaminants is mercury. Despite attempts to curtail Hg use and (by-)production,[3] Hg management is still a major issue in environmental chemistry.[4] Prominent aspects of metal management are identification of sources, determination of the target metal, risk assessment, and removal. Determination of Hg is either done after sampling and cleanup with laboratory-based methods, such as atomic spectroscopy or directly

[a] Dr. J. V. Ros-Lis, R. Casasús, M. Comes, C. Coll, Dr. M. D. Marcos, Prof. R. Martínez-Máñez, Dr. F. Sancenón, Dr. J. Soto
Instituto de Química Molecular Aplicada (IQMA)
Departamento de Química
Universidad Politécnica de Valencia
Camino de Vera s/n, E-46022 Valencia (Spain)
Fax: (+34) 963-879-349
E-mail: rmaez@qim.upv.es.

[b] Prof. P. Amorós, Dr. J. El Haskouri, Dr. N. Garró
Institut de Ciència del Materials (ICMUV)
Universitat de València
P.O. Box 2085, E-46071 València (Spain)
Fax: (+34) 963-543-633
E-mail: pedro.amoros@uv.es.

[c] Dr. K. Rurack
Div. I.5, Bundesanstalt für Materialforschung und -prüfung (BAM)
Richard-Willstätter-Strasse 11
D-12489 Berlin (Germany)
Fax: (+49) 30-8104-5005
E-mail: knut.rurack@bam.de.

  

on site, in situ, or in screening applications. In the last cases, optical and electrochemical sensing devices are mostly employed.[5] In particular, in optical sensors the active part is often an indicator dye that responds to the analyte by a change in colour or fluorescence. Considerable effort has thus been devoted to the development of fluoro- or chromogenic indicator dyes for $Hg^{2+}$.[6–9] Remediation of mercury and other heavy metals, on the other hand, requires potent sorption materials.[10,11] The various materials employed for removal of Hg include polymers, organically modified sol–gel materials, and chitosan.[12,13] In the last decade, following the pioneering works of Liu et al. and Pinnavaia and Mercier,[14,15] organically functionalised mesoporous silica materials have increasingly received attention in this field.[16–18] Recently, such hybrid mesoporous materials have also stimulated areas such as supramolecular chemistry and chemical sensing.[19] Despite the remarkable advances in these two fields, as far as we know, there are no reports on materials that perform dual remediation/signalling functions. With our background in this field,[20,21] we became interested in combining recognition with adsorption chemistry and created a 3D hybrid material with dual functionality for chromofluorogenic detection and removal of $Hg^{2+}$ as proof of concept.

The development of a material for both detection and indication purposes requires a strategy that is distinctly different from the conventional design of molecular probes. Instead, the key requirement for efficient removal of the target dictates the primary design of the hybrid. First, the material must be a potent sorption material. The challenge thus was to integrate a sensitive and selective indication mechanism into a support that is densely covered with binding sites that preferably bind the target with high association constants. Aiming at a system that reports the presence of the target by optical signals, we refrained from utilising the commonly employed "binding site/signalling subunit" approach.[22] Such probes or ionophores usually show reversible responses and often require complex synthetic procedures, so that the equipping a support with a large amount of these supramolecules is not very convenient. From the alternative protocols for $Hg^{2+}$ signalling published in recent years,[23] we opted for the chemodosimeter approach,[24] which we have successfully employed in various cases.[25–28] Chemodosimeters operate through a specific chemical reaction between dosimeter molecule and target species leading to the formation of a fluorescent or coloured product. In contrast to minor modulations or shifts of absorption or emission bands that are often observed for molecular probes based on the binding site/signalling unit approach, chemodosimeters thus exhibit true on/off "switching" behaviour. Several chemodosimeters have been reported for $Hg^{2+}$ indication and they mostly operate through sulfur-elimination reactions.[29] In contrast to the common applications in homogeneous phases,[24,29] we decided to elaborate our approach that relies on an $Hg^{2+}$-induced desulfurisation reaction with concomitant formation of an intensely coloured squaraine derivative,[28] by combining it with the advantageous features of ordered 3D mesoporous silica sorption materials of the MCM41 type,[14–17,30] so that the resulting composite can be used in many different media in a heterogeneous manner for the intended purposes of $Hg^{2+}$ indication and removal.

## Results and Discussion

**Hybrid-material design. The indication reaction**: The design of the colourimetric protocol for $Hg^{2+}$ indication we report herein takes advantage of the favourable features of the chemodosimeter approach. The general protocol is outlined in Scheme 1. The system uses a suitable dye that is first

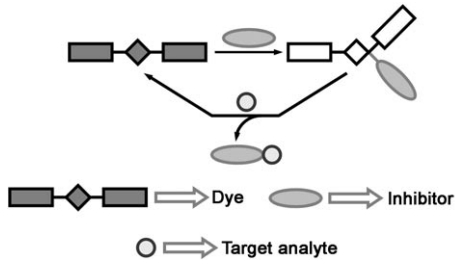


Scheme 1. General $Hg^{2+}$ indication protocol.

"switched off" by a simple addition reaction with a small organic molecule that acts as a "spectroscopic inhibitor". This leuko form of the dye represents the actual chemodosimeter and is colourless and non-fluorescent. In the second step, the target analyte reacts with the inhibitor and the chromophoric $\pi$ system is restored, with reappearance or "switching on" of both colour and fluorescence.

The chemosensor design for selective indication of $Hg^{2+}$ is shown in Scheme 2. The signalling element is squaraine

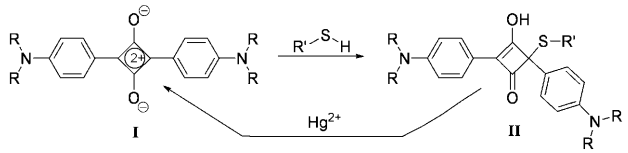


Scheme 2. Chemodosimeter design with squaraine dyes. R is usually an alkyl chain.

dye **I**. Squaraines consist of an electron-deficient central four-membered ring with two substituted aniline moieties attached to the 1,3-positions. They are attractive for chromo- and fluorogenic optical detection,[8,26,27,31] since they have the advantageous features of polymethine dyes, such as an intense absorption band ($\lg \varepsilon > 5$) at long wavelengths and a weakly Stokes shifted fluorescence with comparatively high quantum yields even in aqueous environments.[32] The chemodosimetric leuko form is created in a reversible reaction

  

with an alkyl thiol (the spectroscopic inhibitor) that interrupts the π conjugation in the chromophore by formation of colourless addition product **II**. When the target ion $Hg^{2+}$ is present, this thiophilic analyte induces an elimination reaction in **II** that regenerates the squaraine dye and forms the corresponding $Hg^{II}$ thiolate. As we recently reported in a preliminary communication, this protocol of metal-induced dye release allows sensitive and selective chromo- and fluorogenic detection of $Hg^{2+}$ with simple test strips.[28]

**Implementation of indication and sorption functions**: In our proof of principle utilising a simple test strip, we adsorbed the squaraine dye on a support and passivated it with propanethiol vapour.[28] Dipping the test strips into aqueous solutions containing $Hg^{2+}$ then led to a chemodosimetric reaction in which the strip was transformed from colourless to deep blue and the metal thiolate remained in the sampled solution. Such a strategy is of course not applicable when aiming to indicate and remove the target. Instead, the function responsible for the remediation process must be bound to the support material. Hybrid material **U1** was thus designed in the following way. As mentioned above, the excellent sorption features of mesoporous silica materials and our own favourable experience with these hybrid solids prompted us to rely on these inorganic scaffolds with preorganised structural features and high accessibility of the pores. In particular, we employed mesoporous MCM41-type material UVM-7, which is characterised by a homogeneous distribution of pores about 2–3 nm in diameter and a very large specific surface area of more than $1000\,m^2\,g^{-1}$.[33] UVM-7 consists of MCM-41-type mesoporous nanosized particles joined together in microsized conglomerates with textural porosity in the range of 40–70 nm that has been reported to facilitate movement of active species through the solid.[34] Additionally, these supports can be easily derivatised with a large range of functional groups.[19,35] For comparison, an analogous material **M1** with micrometre-sized MCM-41 particles was prepared (see below).

The selected spectroscopic inhibitor is a thiol group that displays a high affinity for both the dye and the target metal ion. These SH groups are attached to the silica framework by reaction with an alkoxysilane reactant, and aspects such as the degree of functionalisation and choice of solid scaffold are crucial parameters for design of the hybrid.

The preparation of **U1** is shown in Scheme 3. In the first step, mercaptopropyltriethoxysilane (MPTS) was used together with triethanolamine ($TEAH_3$), tetraethyl orthosilicate (TEOS) and cetyltrimethylammonium bromide (CTAB) to prepare a thiol-containing derivative of mesoporous UVM-7 through co-condensation protocols to favour good SH dispersion. The as-prepared solid was then washed with HCl (1 M in ethanol) overnight to remove the surfactant and any excess thiol from the pores to yield UVM-7-SH. This solid consists of a mesoporous MCM41-type support with pore surfaces decorated by thiopropyl groups. Treatment of UVM-7-SH with squaraine derivative **III** in acetonitrile/water (1:5) at pH 9.3 (0.01 M *N*-cyclohexyl-2-aminoethanesulfonic acid, CHES) led to complete bleaching of the solution. A slightly basic pH was selected because the reaction of **III** with the solid is much faster at this pH due to higher nucleophilic character of the sulfur atom as a consequence of deprotonation of the thiol group.[36] The addition reaction between thiol group and squaraine dye produces a 2,4-bis(4-dialkylaminophenyl)-3-hydroxy-4-alkylsulfanylcyclobut-2-enone (APC) derivative that is covalently anchored to the silica matrix. The resulting white solid **U1** was then collected by filtration, washed and dried.

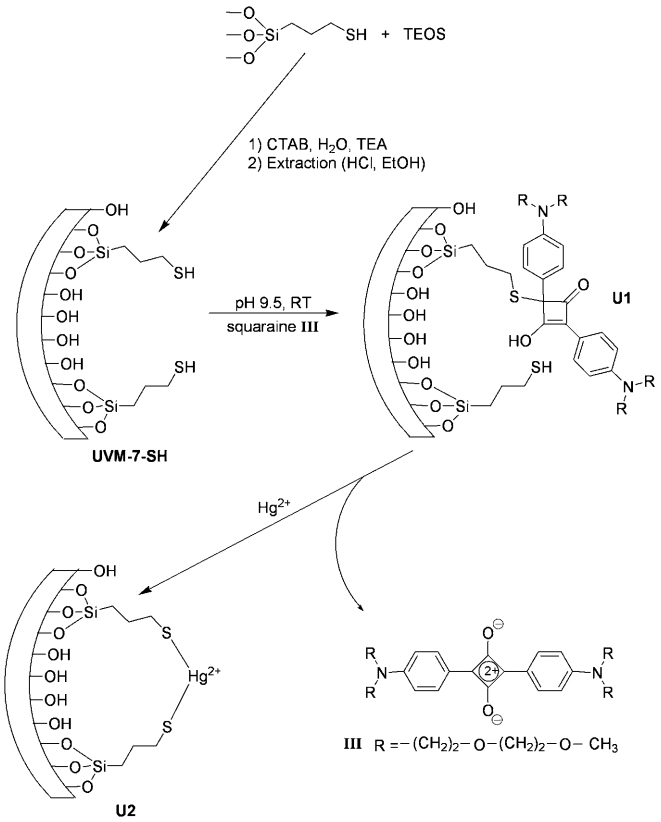


Scheme 3. Route for the preparation of UVM-7-SH, **U1** and **U2**.

In accordance with Scheme 1, in the present case solid UVM-7-SH acts as the spectroscopic inhibitor and **U1** can be considered to be the chemodosimeter. Scheme 3 also shows the expected performance of polyfunctional material **U1**: contact of **U1** with aqueous solutions of $Hg^{2+}$ would result (vide infra) in both uptake of the cation from the solution (like in model solid **U2**) and release of the blue, fluorescent squaraine dye **III** to the solution.[37]

Following this general synthetic route, two solids with different amounts of sulfur atoms were prepared: **U1** containing 2.1 and **U1-8** containing 8.0 wt% of S. Complete material characterisation is given below for **U1**, whereas for **U1-8**, which was only used for comparative purposes in the adsorption experiments (vide infra), standard characterisation methods were applied.

**Reference and model materials**: As described in the Experimental Section, **U2** was prepared as reference material with

  

a loading ratio of thiol/$Hg^{2+}$ = 2:1 and was used for comparative and illustrative purposes in material characterisation. To determine the role that the special mesoporous topology of **U1** and its nanometre-sized particles play in the present application, three model materials were designed. Two were prepared in a similar fashion by using commercially available 2D silicas, micrometre-sized particles of activated silica gel (for **G1**) and fumed silica with nanometric particles (for **F1**) as support. In the first step, the silica support was treated with an excess of MPTS in anhydrous toluene for 3 h. The resulting solids were collected by filtration and washed for 24 h with $CH_2Cl_2$ to remove excess thiol. They were then treated with squaraine **III** to yield the corresponding materials **G1** and **F1**, which lack the mesoporous structure. The third model material **M1** was obtained from micrometre-sized MCM-41 particles by using the same procedure as for the preparation of **U1**. Material **M1** also contains 2.1 wt% of S. This MCM-41 derivative is also a mesoporous solid, but the micrometre-sized particles are much larger than the nanosized particles of the UVM-7-based material **U1**. Thus, non-porous **F1** is comparable in its nanometric particle size to mesoporous **U1**, and non-porous **G1** is comparable in its micrometric particle size to mesoporous **M1**.

**Materials characterisation**: The solids were characterised by standard procedures. X-ray diffraction (XRD) patterns of the hybrid materials UVM-7-SH, **U1** and **U2** (Figure 1)

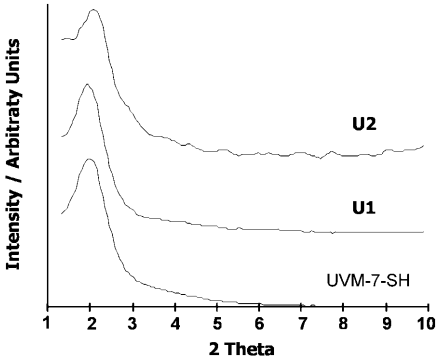


Figure 1. Powder XRD patterns of UVM-7-SH, **U1** and **U2**.

show that the intense peak at about $2\theta = 2°$, characteristic of surfactant-assisted mesoporous materials, does not suffer major changes; that is, the synthetic steps do not significantly affect the mesoporous structure of the silica matrix. In addition to the mesopore system, a bimodal pore array characteristic of UVM-7-like solids can be deduced from transmission electron microscopy (TEM) and porosimetry measurements. Figure 2 depicts a representative TEM image of UVM-7-SH showing the nanoparticulate architecture and the hierarchic bimodal pore organisation that is characteristic for UVM-7 silicas. Figure 2 also shows a TEM image of the MCM-41-SH material with its micrometre-sized architecture. Hybrid material **U1** and mercury-loaded reference material **U2** show similar TEM images (not shown). The $N_2$

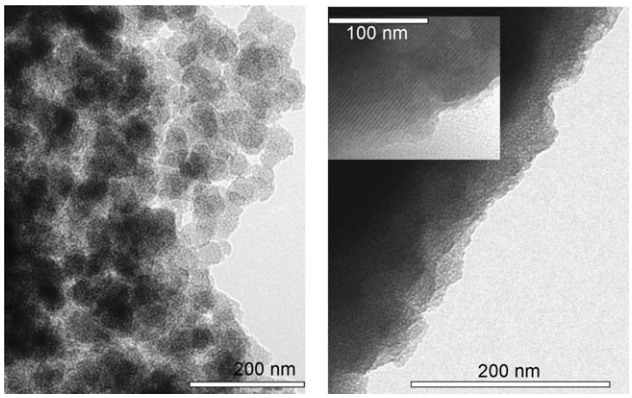


Figure 2. TEM image of UVM-7-SH (left) and MCM-41-SH (right).

adsorption/desorption isotherms (Figure 3) show the expected trend for the mesoporous solids. The isotherm for UVM-7-SH shows two steps. The first, at intermediate relative

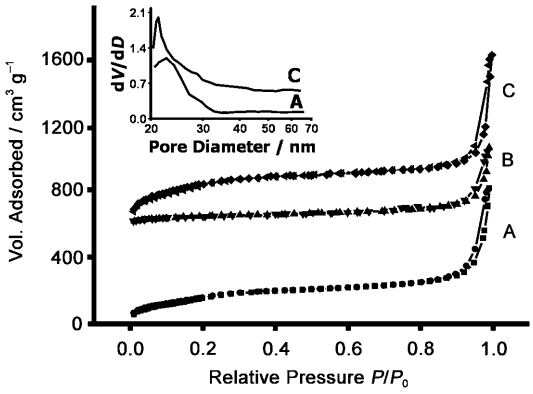


Figure 3. $N_2$ isothermal absorption/desorption curves for A) UMV-7-SH, B) **U1** and C) **U2**. The inset shows the BJH pore size distribution for A) UVM-7-SH and C) **U2**.

pressure ($0.2 < P/P_0 < 0.6$), is related to capillary condensation of $N_2$ in the mesopores. The absence of a hysteresis loop in this interval and a narrow pore distribution suggest the existence of uniform cylindrical mesopores. For this step, an average pore diameter of 2.37 nm and an average pore volume of 0.39 $cm^3 g^{-1}$ were derived. The second step, at higher relative pressures, is associated with filling of textural interparticle pores. In this case, the curves show hysteresis and a broader pore distribution. A volume of 0.99 $cm^3 g^{-1}$ and a diameter of 39.6 nm were determined for the textural pores. For the remaining solids, the specific surface areas, calculated from a Brunauer–Emmet–Teller (BET) treatment of the isotherms,[38] and volumes and the pore sizes, estimated by the Barrett–Joiner–Halenda (BJH) method,[39] are listed in Table 1. Comparison of these data with those of the non-functionalised solid UVM-7 (average mesopore diameter and volume: 2.97 nm, 0.98 $cm^3 g^{-1}$; average textural pore diameter and volume: 66.5 nm, 1.42 $cm^3 g^{-1}$) shows that a relatively high degree of functionalisation in UVM-7-SH re-

  

Table 1. BET specific surface areas, pore volumes and pore sizes calculated from the $N_2$ adsorption/desorption isotherms[a] for selected materials.

| | $S_{BET}$ [$m^2 g^{-1}$] | $V_{text}$[b] [$cm^3 g^{-1}$] | $D_{text}$[b] [nm] | $V_{meso}$[c] [$cm^3 g^{-1}$] | $D_{meso}$[c] [nm] |
|---|---|---|---|---|---|
| UVM-7[d] | 1075 | 1.42 | 66.5 | 0.98 | 2.97 |
| UVM-7-SH | 596 | 0.99 | 39.6 | 0.39 | 2.37 |
| **U1** | 177 | 0.64 | 40.7 | 0.11 | –[e] |
| **U2** | 626 | 0.81 | 46.6 | 0.41 | 2.52 |
| **G1** | 389 | 0.52 | 5.4 | – | – |
| MCM-41-SH | 444 | – | – | 0.28 | 2.50 |
| **M1** | 149 | – | – | 0.10 | –[e] |

[a] $P/P_o = 0.6$ was taken as the limit to separate mesoporous filling from textural pore filling. [b] Volume $V$ and diameter $D$ of textural pore. [c] Volume $V$ and diameter $D$ of mesopore. [d] Values taken from ref. [34a]. [e] No reliable values could be obtained.

Table 2. Thiol and APC contents and estimated average coverage for selected materials.

| | Thiopropyl[a] [$mmol g^{-1}$] | APC[a] [$mmol g^{-1}$] | $\beta_{Thiol}$[b] [$thiol nm^{-2}$] |
|---|---|---|---|
| UVM-7-SH | 0.94 | – | 0.52 |
| **U1** | 0.95 | 0.01 | 0.53 |
| **U2** | 0.93 | – | 0.52 |
| **G1** | 0.75 | 0.01 | 0.90 |
| MCM-41-SH | 0.89 | – | 0.53 |
| **M1** | 0.87 | 0.002 | 0.53 |

[a] Thiol and APC groups in millimoles per gram of $SiO_2$. [b] Thiol molecules per surface unit.

duces the sizes of both textural and mesopores. In the case of **U1**, which contains the chemodosimeter moieties, the first step in the $N_2$ adsorption/desorption isotherms that corresponds to the filling of the mesoporous is virtually absent, because of the high saturation of the pores with APC groups. Only the larger textural pores can be traced (average textural pore diameter and volume: 40.7 nm, 0.64 $cm^3 g^{-1}$). A similar trend was observed for the micrometric MCM-41-based materials (see Table 1). The endpoint of performance that can be expected is evident from the data for **U2**. Coordination of mercury and elimination of the thiol–squaraine adduct with subsequent washing out, as described in the Experimental Section, results in opening of the mesopores, and both the pore volume and diameter are retrieved (see below).

The infrared spectra of solids **U1**, **G1**, **F1** and **M1** show the expected features, that is, intense bands due to the silica matrix (1250, 1087, 802, 462 $cm^{-1}$), vibrational bands of water molecules (3420 and 1620 $cm^{-1}$) and vibrational bands of C–H bonds of the anchored organic moieties (2954–2850 $cm^{-1}$). The presence of thiol groups could not be unambiguously confirmed, as the vibrations of the $HSCH_2$ group result in very weak bands.

A central issue for the performance of the solids is to equip them with an optimum amount of squaraine (APC groups) on the silica surface. As explained above, the squaraine is anchored to the silica surface by reaction of the thiol-containing solid with a solution of **III** in acetonitrile. For the target material **U1**, different concentrations of squaraine were tested, and the optimum loading was obtained by treatment of the material (300 mg) in acetonitrile/water (1:5, 120 mL) at pH 9.3 (0.01 M CHES) with a solution of **III** in acetonitrile (1.3 mL, 1.5 mM; Table 2). Assuming that decolouration of the squaraine solution, whether partial or total, is only due to the reaction with the thiol groups, the total amount of APC anchored to a certain solid can be calculated (cf. Scheme 3 and Table 2). Optimum loading was judged by the uptake rate of **III** and the absence of residual colour in the solid. For **U1**, the optimum amount of **III** does not correspond to the maximum loading possible, because our intention was to create a reusable material (i.e., with optimum uptake rate for fast regeneration) and to avoid adsorption of unconverted squaraine in the pores (i.e., have a bleached material without traces of blue squaraine absorption). The latter point is important in the effort to avoid leaching of residual unconsumed squaraine into the solution to give false positive signals. Under the same conditions as used for **U1**, MCM-41-SH was unable to completely bleach the blue solution. Thus, for **M1**, the amount of APC given in Table 2 corresponds to the maximum (and optimum) loading. For fumed silica and silica-gel derivatives, two materials each prepared with 1) the same amount of **III** as used for **U1** (**F1** and **G1**) and 2) five times more **III** (**F1-5** and **G1-5**). Both **F1** and **F1-5** as well as **G1** and **G1-5** showed similar performance (see below). A special feature of significance for results below is that, despite the presence of a similar amount of SH groups, **U1** contains a remarkably larger amount of APC groups in its optimised form than **M1** with maximum APC loading (0.01 vs. 0.002 mmol APC per gram of $SiO_2$, respectively). To understand this different loading of APC moieties for the two mesoporous solids it is important to recall two distinctive features. First, **U1** and **M1** have different natures on the nanometric scale. Whereas the UVM-7 derivative consists of conglomerates of nanosized particles, the MCM-41 derivative is characterised by the presence of micrometre-sized particles. This implies that the pore length is notably shorter for **U1** compared with **M1** (a few nanometres vs. several micrometres). The second important point is related to the size of squaraine **III** (ca. 25 Å), which is large enough to partly block the pores (e.g., see Table 1). This in agreement with reports on post-synthetic grafting of mesoporous materials, which commonly leads to anchoring of the products inside the channels, but close to the pore openings, especially for large molecules.[40] Both features, that is, partial pore blockage with APC groups and very different pore lengths, support our findings that the number of APC groups in **U1** is significantly larger than that in **M1**. In fact, such a dependence of loading capacity on the pore length has not only been described for UVM-7 materials when compared with typical MCM-41 supports,[41] but also for other mesoporous scaffolds; the loading increases with decreasing pore length.[42]

The degree of functionalisation of the solids was also assessed by elemental analysis and thermogravimetric studies. From the elemental contents (C, H, N, S), the amount of

  

thiol and APC groups contained in the materials were calculated in millimole per gram of $SiO_2$ (mmol $g^{-1}$ $SiO_2$) by using Equation (1)

$$\alpha_A = \frac{\Delta W_i \times 1000}{\Delta W_{SiO_2} \times nM_i} \quad (1)$$

in which $\Delta W_i$ ($i$=N, S, C) are the weight percentages of carbon, nitrogen or sulfur, $M_i$ is the corresponding atomic weight, $n$ the number of corresponding atoms in one molecule and $W_{SiO_2}$ the inorganic $SiO_2$ content in weight percent. These experiments show that the amount of organic material increases from UVM-7-SH and MCM-41-SH to **U1** and **M1**, because of the reaction of the former solids with the squaraine dye.[43] Materials UVM-7-SH and MCM-41-SH contain 0.94 and 0.89 mmol of thiol groups per gram of $SiO_2$, respectively. This content remains the same in APC-functionalised **U1** (0.95 mmol $g^{-1}$ $SiO_2$), **M1** (0.87 mmol $g^{-1}$ $SiO_2$) and also in fully $Hg^{2+}$ loaded **U2** (0.92 mmol $g^{-1}$ $SiO_2$); that is, the covalently bound thiol groups are not affected by either preparation of the chemodosimeter or by the sorption process (vide infra).

Taking into account these contents and the value of the specific surface of the UVM-7 support, the average coverage ($\beta_A$ in groups per square nanometre) of the surface of the different solids by thiol groups was calculated by Equation (2)

$$\beta_A = \alpha_A \times 10^{-3} \times S^{-1} \times 10^{-18} \times N_A = \alpha_A \times S^{-1} \times 602.3 \quad (2)$$

in which $\alpha_A$ is the thiol content (mmol $g^{-1}$ $SiO_2$), $S$ the specific surface area ($m^2 g^{-1}$) of (non-functionalised) UVM-7 or MCM-41 and $N_A$ the Avogadro number (Table 2). From Equation (2) a surface coverage of about 0.53 thiol groups per square nanometre was calculated for the UVM-7 and MCM-41 derivatives, which results in an average interthiol distance of 13.7 Å for these solids. As we discuss below, this average thiol–thiol distance is compatible with the formation of $Hg^{2+}$ dithiolate complexes.

**Hybrid-material performance—indication of $Hg^{2+}$**: Composite **U1** contains the squaraine dye in its leuko APC form attached to the mesoporous UVM-7-type solid support. Addition of the thiol groups to the four-membered squaric ring of the dye molecules results in transformation of the intensely coloured squaraine derivative into the colourless APC, because the polymethinic electron delocalisation in the squaraine framework is interrupted. As we recently reported,[28] APC consists of two independent subchromophores that are electronically separated by an $sp^3$-hybridised carbon atom and thus absorb in the UV spectral region. Accordingly, the absorption spectrum of **U1** only shows a poorly resolved band in the UV region that corresponds to the two subchromophores, that is, the dialkylanilino- and dialkylaminophenylhydroxy-4-alkylsulfanylcyclobut-2-enone moieties. The absence of the typical squaraine absorption band at about 620 nm stresses the fact that no squaraine was adsorbed onto the surface of the solid during the preparation of **U1**.

The performance of **U1** as a chromofluorogenic indicator for $Hg^{2+}$ was studied as follows. In a typical experiment, 5 mg of **U1** was added to solutions containing 1 mM of the corresponding metal in acetonitrile/water (1:1) at pH 3.[36] Pure water was not used in order to enhance the solubility of the squaraine derivative at high concentrations of mercury. However, for experiments with a lower delivery of the squaraine dye, pure water can be used. After two minutes of reaction, the solid was collected by filtration, and the absorbance of the resulting solution monitored. As expected, addition of **U1** to solutions containing $Hg^{2+}$ ions resulted in a rapid and dramatic change of the colour from colourless to deep blue due to the appearance of a new and intense absorption band at 642 nm that is typical for a squaraine dye (Figure 4). The solution also shows remarkable fluorescence.

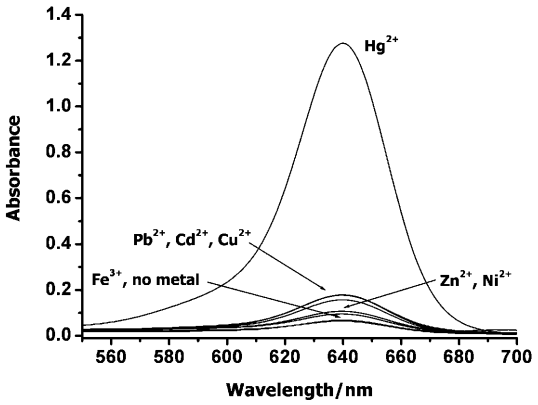


Figure 4. Absorption spectra of **U1** in the presence of selected metal ions ($[M^{n+}]$=1 mM) in acetonitrile/water (1:1) at pH 3.0.

This dual switching-on of chromo- and fluorogenic sensing of $Hg^{2+}$ is in agreement with the reaction depicted in Scheme 3. The response is noteworthy since both absorption and emission are found at the far end of the visible spectral window at which interference due to matrix absorption or autofluorescence of the sample is usually negligible. Additionally, this dramatic hyper- and bathochromic shift on mercury-induced release of **III** allows straightforward naked-eye detection of $Hg^{2+}$ by an easy-to-use procedure.

Coordination with thiols can also take place with other metal ions, and therefore the cross-reactivity of **U1** with $Pb^{2+}$, $Ni^{2+}$, $Cd^{2+}$, $Zn^{2+}$, $Cu^{2+}$ and $Fe^{3+}$ was tested in a similar fashion (Figure 4). Besides the remarkably selective response to $Hg^{2+}$, the presence of other thiophilic cations such as $Pb^{2+}$ and $Cd^{2+}$ only leads to very minor dye release at relatively high concentrations of 1 mM. In the presence of all the other cations, **U1** remained silent. Moreover, **U1** shows no response to the presence of alkali and alkaline earth metal ions or to anions ubiquitously present in water, such as chloride, carbonate, sulfate and phosphate. Figure 5 shows the dye liberation observed for **U1** as a function of

  

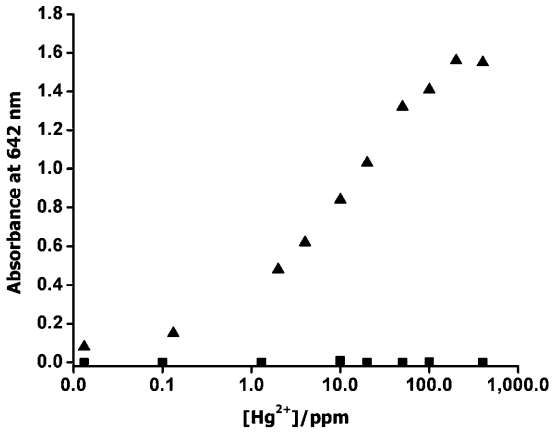


Figure 5. Absorbances at 642 nm of **U1** (triangles) and **G1** (squares) as a function of $Hg^{2+}$ concentration in acetonitrile/water (1:1) solutions at pH 3.0.

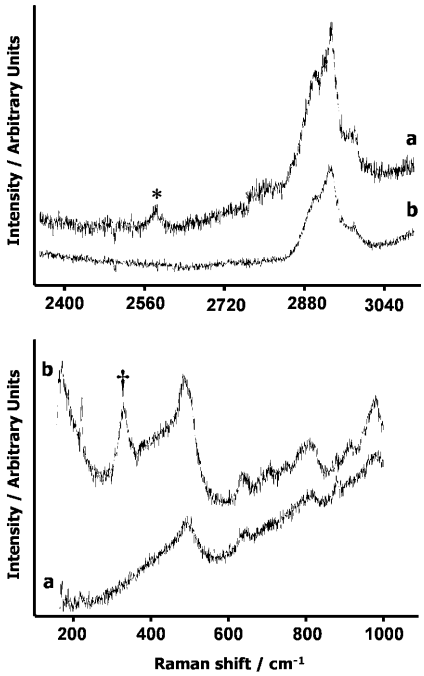


Figure 6. High- (top) and low-energy (bottom) domains of the Raman spectra of a) **U1** and b) **U2**; ∗ ν(S–H) and † ν(S–Hg) bands.

increasing amounts of $Hg^{2+}$. Mesoporous solid **U1** shows a remarkable chromogenic response to the presence of $Hg^{2+}$ over a large dynamic concentration range with an apparent detection limit of about 0.1 ppm for colourimetric analysis. Apparent detection limit here means that, since the ratio of thiol to APC groups is 95:1 (Table 2), statistically only about 2% of the 0.1 ppm of $Hg^{2+}$ reacts with the APC groups, that is 2 ppb $Hg^{2+}$ is sufficient to generate a well-exploitable absorption signal. As shown previously,[28] the detection limit can be lowered by fluorescence detection.

**Removal of $Hg^{2+}$—tracing the step from U1 to U2**: We studied the transformation of sensor material **U1** after reaction with $Hg^{2+}$. First, solid **U2** was prepared by treating **U1** with a stoichiometric amount of $Hg^{2+}$ to give the 1:2 (Hg:S) solid. Elemental and thermogravimetric analyses showed that the amount of thiol groups per gram of $SiO_2$ in **U1** and **U2** remains unaltered, that is, the reaction of **U1** with $Hg^{2+}$ occurs by uptake of metal cations from solution and delivery of the anchored squaraine derivative from the pore voids into the aqueous solution. The N and C contents increase from UVM-7-SH to **U1**, in agreement with formation of the APC derivative. In contrast, addition of $Hg^{2+}$ to **U1** reduces the N content to nearly zero, indicative of almost quantitative delivery of the squaraine to the solution. This reduction in the organic loading is reflected by changes in the mesoporous structure, that is, the 2 nm mesopores that were lost in **U1** are recovered in **U2** (Table 1).

At the mesoscopic level, XRD, TEM and $N_2$ adsorption/desorption isotherm measurements on **U2** confirmed preservation of the UVM-7 architecture from UVM-7-SH via **U1** to $Hg^{2+}$-loaded **U2**. The question now remains whether the mechanism proposed in Scheme 3, namely, formation of $Hg^{2+}$ dithiolate complexes, is valid. For this purpose, the Raman spectra of **U1** and **U2** were recorded (Figure 6). We focussed on two spectral regions, around 2500 $cm^{-1}$, at which the unperturbed thiol groups should exhibit a well-expressed S–H stretching vibration, and between 180–400 $cm^{-1}$, the typical spectral domain of Raman-active Hg–S stretching vibrations for $Hg^{2+}$ thiolates in both solution and the solid state.[44]

The Raman spectra in Figure 6 confirm the presence of free SH groups for **U1**, since a small band is detected at 2580 $cm^{-1}$. However, this band completely disappears after reaction with $Hg^{2+}$ (**U2**). Hence, as proposed in Scheme 3, all thiol groups in **U2** remain connected to $Hg^{2+}$ species. On the other hand, the low-energy Raman region of Figure 6 shows a well-resolved and non-split band at 328 $cm^{-1}$ for **U2** that can be attributed to the existence of twofold coordinated -S-Hg-S- ($Hg^{2+}$:thiol = 1:2) complexes.[44] The position of Hg–S stretching modes strongly depends on the coordination number of mercury, and only atoms which are strongly bound to mercury (average bond length $<0.28$ nm) influence the relevant vibrational modes; this supports our present assignment. The average thiol–thiol distance of 13.7 Å is compatible with the formation of $Hg^{2+}$ dithiolate complexes. Assuming an all-*trans* configuration of the organic moiety and typical Si–C, C–C, C–S and Hg–S distances, mercury centres can bind thiol groups that are separated by up to about 15.2 Å. In addition, the concave surface inside the mesopores should favour formation of $Hg^{2+}$ dithiolate complexes due to a certain reduction of the thiol–thiol distances.

**Importance of the ordered porous structure for sensing. U1 versus G1 and F1**: The Raman data already hint at the important role played by the mesoporous structure of material **U1**. The inorganic skeleton not only acts as an innocent support, but also plays an active role in the sensing/removal

  

processes.[19] A comparative investigation of **U1** with **G1** and **F1** furnished additional support for this conclusion. Materials **G1** and **F1** were prepared from 2D silica materials and are thus analogous to **U1**, but do not have a mesoporous structure. The specific surface areas of the parent materials are distinctly lower (ca. 500 and ca. 200 $m^2 g^{-1}$ for silica gel and fumed silica, respectively). Although the sulfur content per gram of $SiO_2$ is lower in **G1** (0.75 $mmol g^{-1}$ $SiO_2$) and **F1** (0.14 $mmol g^{-1}$ $SiO_2$) than in **U1** (0.95 $mmol g^{-1}$ $SiO_2$), the last-named solid has a higher specific surface area (UVM-7: ca. 1000 $m^2 g^{-1}$) than the other two, and therefore the numbers of millimoles of sulfur atoms per square nanometre are comparable for **F1** and even larger for **G1** (0.90, 0.44 and 0.53 for **G1**, **F1** and **U1**, respectively). The response of **G1** toward $Hg^{2+}$ (Figure 5) shows that it is a very poor $Hg^{2+}$ indicator even in the presence of a large excess of metal ions.[45] The same is found for **F1**. Additionally, equipping both 2D materials with larger amounts of APC does not improve the response, that is, **F1-5** and **G1-5** also do not deliver a sizeable amount of squaraine to the solution.

We tentatively ascribe the different responses of **U1** and **G1**/**F1** to the different structures of the solids. The presence of nanoscopic channels in **U1** in which the proximal thiol groups are located at a concave surface seems to facilitate much better binding of the target than the rather flat surfaces of the 2D materials, which can locally also be very inhomogeneous with flat, convex, and concave microdomains for **F1**. The geometry of the solid substrate may influence the packing and molecular ordering in the anchored monolayer and thus affect surface-related properties of the materials.[46] This is in agreement with reports of Liu et al., who found a considerably lower adsorption capacity of thiol-functionalised silica gel supports (2D surfaces) for $Hg^{2+}$ compared to thiol-containing mesoporous structures (3D surfaces).[14] Apparently, once $Hg^{2+}$ enters the pores, it reacts more readily with the APC moieties in the confined space, and this results in more efficient release of the squaraine dye to the solution. The much less effective $Hg^{2+}$ binding on "flat" surfaces reflects the synergetic effect of the multifunctional hybrids for improved signalling and sorption.

**Performance of U1 in $Hg^{2+}$ adsorption**: The performance of **U1** as an adsorbent distinguishes it from other, conventional $Hg^{2+}$ probe molecules reported so far. Since **U1** not only contains free thiol groups like other thiol-containing mesoporous materials that were recently designed as heavy-metal adsorbents for environmental remediation,[14–18] but also S atoms that are anchored to the APC fragment (Scheme 3), the central question was whether **U1** is as potent a sorbent for $Hg^{2+}$ as it is a chemodosimeter for this ion.

The adsorption capacity of **U1** was studied under the same conditions as employed for the sensing experiments (see above). Two derivatives **U1** and **U1-8**, respectively containing about 2.1 and 8.0 wt % S, were used for the removal experiments.[47] In a typical test, the material (5 mg) was added to acetonitrile/water (1:1, 5 mL) solutions containing different concentrations of $Hg^{2+}$, and the mixture was stirred at room temperature for 10 min. The suspension was filtered and the $Hg^{2+}$ concentration was determined by standard atomic absorption spectroscopy (see Experimental Section for details). Figure 7 shows the $Hg^{2+}$ adsorption isotherms for **U1** and **U1-8**. For each solid, metal adsorption increases with increasing $Hg^{2+}$ concentration in the solution. In addition, the capacity for the removal of $Hg^{2+}$ is also enhanced for the sulfur-rich material. Saturation is finally reached at about 0.7 and 1.7 mmol of $Hg^{2+}$ per gram of adsorbent for **U1** and **U1-8**, respectively. This adsorption capacity agrees with other studies published on mercury removal by mesoporous functionalised MCM-41-type materials in the literature,[11] that is, the presence of the APC groups in the solid does not significantly affect the high adsorption capability of the mesoporous S-containing matrix. Similar experiments demonstrated that the non-functionalised material UVM-7 adsorbs negligible amounts of $Hg^{2+}$ (not shown).

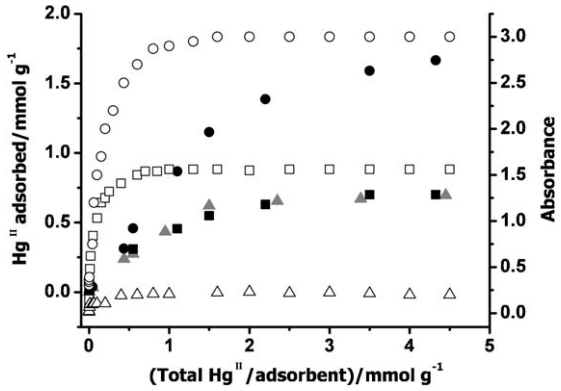


Figure 7. $Hg^{2+}$ adsorption isotherms at pH 3 and 25 °C (full symbols) and colourimetric response (open symbols) for **U1** (squares), **U1-8** (circles) and **M1** (triangles).

The dual functionality of **U1** is summarised in Figure 7, which plots the results of both conducted $Hg^{2+}$-removal and dye-delivery experiments. It is worth noting that the dye-delivery curves shows a steeper slope than the $Hg^{2+}$-uptake curves: while the maximum of absorbance is reached at $Hg^{2+}$ concentrations that correspond to a 1:2 (Hg:S) stoichiometry, the adsorption capacity of both solids still keeps increasing. In fact, if we relate the total amount of adsorbed mercury with the sulfur content of each material we find Hg:S molar ratios of 1.12 and 0.67 for **U1** and **U1-8**, respectively. This means that the maximum amount of metal that can be adsorbed is well above that needed for the formation of the 1:2 complexes and complete dye release. Hence, although it seems that mercury adsorption takes place through formation of 1:2 complexes, this process continues until full mercury loading is reached when the concentration of $Hg^{2+}$ is further increased, especially for the material with the lower sulfur content. These results are in accordance with previous work of Bibby and Mercier.[48] Concerning the suit-

  

ability of both materials for our present purposes, **U1** performs better than **U1-8**, not only because the adsorption of $Hg^{2+}$ per S atom is higher, but also because a lower limit of detection can be reached with **U1**, presumably due to the fact that **U1-8** has a higher thiol-to-APC group ratio.

**Nanoscopic U1 versus microscopic M1 particles**: We compared the performance of two similarly structured mesoporous solids that have different particle sizes, that is, **U1**, based on UVM-7, and **M1** with a typical MCM-41 structure. Whereas the former consists of nanosized particles, the MCM-41 derivative is characterised by the presence of micrometric particles. The adsorption and sensing capabilities were studied under the same conditions as described above. Similar to **U1**, the adsorption capability of **M1** increases with increasing $Hg^{2+}$ concentration (see Figure 7). Both **U1** and **M1** have a similar SH content and therefore both show a rather similar adsorption capability. However, **U1** and **M1** show very different sensing abilities. Whereas **U1** leads to squaraine absorbances of up to 1.5 in the presence of $Hg^{2+}$ under the conditions employed for Figure 7, an analogous amount of **M1** liberates squaraine molecules only up to maximum absorbances of 0.2–0.3. This significantly lower response is clearly associated with the smaller amount of APC groups anchored to **M1** than to **U1**, as a consequence of different loading capacities described above (Table 2). In summary, both **U1** and **M1** show similar behaviour in terms of adsorption ability, but **U1** displays a more sensitive response in the presence of $Hg^{2+}$ ions, which stresses the importance of the textural (nano- versus microscale) shape of the particulate material for dual signalling/adsorption performance when using mesoporous supports. As the experiments with **F1** and **G1** discussed above revealed, the particle size itself is not a decisive criterion here.

Material **U1** can be partially regenerated by simple washing with concentrated HCl, which quantitatively removes the loaded mercury. This transforms **U2** back into UVM-7-SH, which is then ready for regeneration of the chemodosimeter by reaction with squaraine derivative **III**. Figure 8 shows a plot of the adsorption capacity of **U1** over two successive cycles comprising 1) washing with HCl (10 mL of 12 M HCl for 100 mg of solid), 2) loading with squaraine dye and 3) adsorption of $Hg^{2+}$ (solutions of 2.2 mmol of Hg per gram of $SiO_2$).

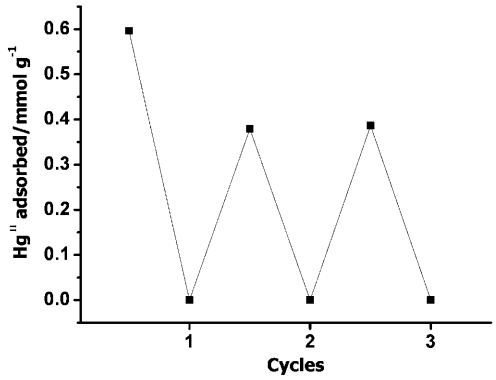


Figure 8. Mercury adsorption capacity of solid **U1** after several cycles of washing with HCl.[49]

The additional possibility of shaping UVM-7 derivatives as monoliths is very appealing for future practical applications of mesoporous materials in adsorption and signalling. As far as we know, **U1** is the first example of a new class of polyfunctional hybrid supports that can be used as both remediation and alarm systems through selective signalling and removal of target species of environmental relevance. Motivated by these favourable features, we are currently carrying out further studies to optimise the loading and sensing abilities of other functional hybrid systems toward different toxic targets.

## Conclusion

We have designed a simple 3D hybrid material with dual functionality for $Hg^{2+}$ detection and adsorption. Signalling is based on a specific reaction in which $Hg^{2+}$ triggers the formation of a highly coloured and highly fluorescent squaraine dye. This results in true switching-on behaviour with the development of a highly fluorescent blue colour from colourless solutions. Besides $Hg^{2+}$ indication, the solid is also able to remove $Hg^{2+}$ ions from aqueous solutions and can be easily regenerated. We believe that the combination of the "chemodosimeter" approach from the field of chemical signalling with the directed design of hybrid supports containing binding sites for selective coordination of toxic metal ions or anions is a very promising route to new and improved polyfunctional materials that allow monitoring of the progress of removal of toxicants without other external devices.[50]

## Experimental Section

**Materials**: All commercially available reagents were used without further purification. Air- and water-sensitive reactions were performed in flame-dried glassware under argon. The synthesis of squaraine derivative **III** has been published elsewhere.[27]

**Physical measurements**: X-ray powder diffractograms were recorded on a Seifert 3000TT diffractometer with $Cu_{K\alpha}$ radiation. Thermogravimetric analyses were carried out on a TGA/SDTA 851e Mettler Toledo balance, with a heating program consisting of a heating ramp of 10 °C per minute from 393 to 1273 K and an isothermal heating step at this temperature over 30 min. IR spectra were recorded on a Jasco FT/IR-460 Plus between 400 and 4000 $cm^{-1}$ in KBr pellets. TEM images were obtained on a Philiphs TEM CM10 operating at 100 kV. $N_2$ adsorption/desorption isotherms were recorded on a Micromeritics ASAP2010 automated sorption analyser. The samples were degassed at 120 °C under vacuum overnight. The specific surface areas were calculated from the isotherm data in the low-pressure range by using the BET model. Pore sizes were determined by following the BJH method for adsorption isotherms. Spectrophotometric measurements were carried out with a Lambda 35 UV/Vis Spectrometer from Perkin–Elmer Instruments. Raman measurements were performed with a Jobin-Yvon T64000 confocal micro-Raman spectrometer equipped with a nitrogen-cooled charge-coupled device detector. The 488 nm line of an $Ar^+$ laser was used for excitation. An edge filter reject-

  

ed the elastic scattering, and the Raman signal was analysed by the third grating of the spectrometer. A 100× microscope objective was used to focus the laser light on the sample to a spot with a diameter of 1 μm. The data were recorded at room temperature in backscattering geometry.

**Preparation of UVM-7-SH**: The synthetic procedure is based on the "atrane route"[30] for the preparation of MCM-41 type materials. This method uses ligands related to triethanolamine ($TEAH_3$; i.e., in general "atranes", and "silatranes" for the silicon containing complexes) as hydrolytic inorganic precursors and surfactants as porogenic species. In a typical synthesis leading to UVM-7 with a homogeneous monolayer of mercaptopropyltriethoxysilane (MPTS, 5%), the molar ratio of the reagents in the mother liquor was fixed to $TEAH_3$/TEOS/MPTS/CTAB/$H_2O$=7:1.90:0.10:0.52:180. Hence, $TEAH_3$ (80.54 g, 0.540 mol), tetraethyl orthosilicate (TEOS, 33.40 mL, 0.147 mol) and MPTS (2.33 mL, 0.008 mol) were added to a round-bottomed flask connected to a Dean–Stark trap under inert atmosphere (Ar gas). The mixture was heated to 140 °C to remove ethanol formed during the formation of the atrane complexes by distillation. Then the mixture was cooled to 90 °C and CTAB (14.62 g, 0.040 mol) was slowly added. Finally, water (250 mL, 13.889 mol) was added and the mixture was subsequently aged at room temperature for 24 h. The resulting powder was collected by filtration, washed with water and ethanol and dried in air. To remove the surfactant, the mesostructured solid was suspended in 1 M HCl in EtOH (1 g of solid per 100 mL of HCl/EtOH) for 1 d at 80 °C. After filtration, the white solid was first washed with distilled water until pH 5–6 and then with ethanol. The solid was finally dried at 70 °C.

**Preparation of U1**: UVM-7-SH (300 mg) was suspended in water/acetonitrile (120 mL, 5/1 v/v, pH 9.6 and 0.01 M *N*-cyclohexyl-2-aminoethanesulfonic acid buffer (CHES)) and a blue solution of squaraine dye (1.3 mL, 1.5 mM) was added. Vigorous stirring of the mixture led to a complete bleaching of the solution. The powder was collected by filtration, washed with acetonitrile and dried at 70 °C to yield **U1**.

**Preparation of U2**: A solution of $Hg^{2+}$ in acetonitrile (15 mL, 5 mM, 0.075 mmol $Hg^{2+}$ as mercury(II) trifluoromethanesulfonate) was added to a suspension of **U1** (150 mg, corresponding approximately to 0.140 mmol of thiol groups) in a mixture of water (75 mL) and acetonitrile (60 mL; final water:acetonitrile 1:1, pH 3) and stirred vigorously. After a few minutes the solution turned blue. The white solid was collected by filtration, washed with acetonitrile and dried at 70 °C to yield **U2**. The absorption spectrum of the mother solution showed an intense band at 642 nm indicative of squaraine **III**.

**Preparation of G1 and F1**: Common silica gel (1 g, average particle size ca. 40–63 μm), previously dried at 120 °C for two hours, was added to a solution of MPTS (5 mL) and toluene (50 mL) under an inert atmosphere. The suspension was heated at 100 °C for 12 h and the powder was collected by filtration, exhaustively washed with toluene and acetone and dried. Excess thiol was then removed by Soxhlet extraction with dichloromethane for 24 h to yield a white powder. Subsequently, this solid (300 mg) was suspended in water/acetonitrile (120 mL, 5:1 v/v, pH 9.6, 0.01 M CHES), and a blue solution of squaraine dye (1.3 mL, 1.5 mM) was added. Vigorous stirring of the mixture led to complete bleaching of the solution. The powder was collected by filtration washed with acetonitrile, and dried at 70 °C to yield **G1**. In a similar way, hybrid nanomaterial **F1** was prepared by using commercially available fumed silica (activated with HCl, average particle size 0.014 μm) instead of silica gel.

**Preparation of MCM41-SH**: The MCM-41 mesoporous support was synthesised by following the so-called atrane route.[30] In a typical synthesis leading to MCM-41 with a homogeneous monolayer of MPTS (5 mol%), the molar ratio of the reagents in the mother liquor was fixed to $TEAH_3$/TEOS/MPTS/CTAB/NaOH/$H_2O$=7:1.90:0.10:0.52:0.55:180. Hence, $TEAH_3$ (80.58 g, 0.540 mol), sodium hydroxide (1.684 g, 0.042 mol), TEOS (33.40 mL, 0.147 mol) and MPTS (2.33 mL, 0.008 mol) were added to a flask. The mixture was heated to 120 °C to remove ethanol released during formation of the atrane complexes. Then, cetyltrimethylammonium bromide (CTAB, 14.62 g, 0.040 mol) was slowly added. Finally, the liquid was cooled to 70 °C and then water (250 mL, 13.89 mol) was added with vigorous stirring. The mixture was subsequently aged at room temperature for 24 h. The resulting powder was collected by filtration, washed with water and ethanol and dried in air. To remove the surfactant, the mesostructured solid was treated as described for UVM-7-SH.

**Preparation of M1**: Solid MCM-41-SH (300 mg) was treated according to the same procedure as used for **U1**.

## Acknowledgements

We thank the Ministerio de Ciencia y Tecnología (FEDER projects CTQ2006-15456-C04-01 and CTQ2006-15456-C04-03) for financial support and the personnel of the Electron Microscopy Service at the Universidad Politécnica de Valencia for technical support. J.V.R.L. also thanks the Generalitat Valenciana for a postdoctoral fellowship.

[1] L. D. Hylander, M. Meili, *Crit. Rev. Environ. Sci. Technol.* **2005**, *35*, 1–36.
[2] R. P. Mason, W. F. Fitzgerald, F. M. M. Morel, *Geochim. Cosmochim. Acta* **1994**, *58*, 3191–3198; O. Lindqvist, *J. Power Sources* **1995**, *57*, 3–7.
[3] L. D. Hylander, *Water Air Soil Pollut.* **2001**, *125*, 331–344.
[4] a) A. B. Mukherjee, R. Zevenhoven, J. Brodersen, L. D. Hylander, P. Bhattacharya, *Resour. Conserv. Recycl.* **2004**, *42*, 155–182; b) S. P. Mohapatra, I. Nikolova, A. Mitchell, *J. Environ. Manage.* **2007**, *83*, 80–92.
[5] a) I. Oehme, O. S. Wolfbeis, *Mikrochim. Acta* **1997**, *126*, 177–192; b) R. Martínez-Máñez, J. Soto, J. M. Lloris, T. Pardo, *Trends Inorg. Chem.* **1998**, *5*, 183–203; c) I. Palchetti, G. Marrazza, M. Mascini, *Anal. Lett.* **2001**, *34*, 813–824; d) X. M. Meng, L. Liu, Q. X. Guo, *Huaxue Jinzhan* **2005**, *17*, 45–54; e) X. D. Xie, D. Stueben, Z. Berner, *Anal. Lett.* **2005**, *38*, 2281–2300; f) L. Xu, R. Yuan, Y.-Q. Chai, *Chem. Lett.* **2005**, *34*, 440–441; g) V. K. Gupta, S. Chandra, H. Lang, *Talanta* **2005**, *66*, 575–580; h) S. S. M. Hassan, W. H. Mahmoud, A. H. K. Mohamed, A. E. Kelany, *Anal. Sci.* **2006**, *22*, 877–881.
[6] Recent representative examples of fluorescent $Hg^{2+}$ indicators in aqueous and mixed aqueous solution: a) R. R. Avirah, K. Jyothish, D. Ramaiah, *Org. Lett.* **2007**, *9*, 121–124; b) E. M. Nolan, M. E. Racine, S. J. Lippard, *Inorg. Chem.* **2006**, *45*, 2742–2749; c) J. Wang, X. Qian, *Chem. Commun.* **2006**, 109–111; d) X.-M. Meng, L. Liu, H.-Y. Hu, M.-Z. Zhu, M.-X. Wang, J. Shi, Q.-X. Guo, *Tetrahedron Lett.* **2006**, *47*, 7961–7964; e) S. Ou, Z. Lin, C. Duan, H. Zhang, Z. Bai, *Chem. Commun.* **2006**, 4392–4394.
[7] Recent representative examples of colourimetric $Hg^{2+}$ indicators in aqueous and mixed aqueous solution: a) S. Tatay, P. Gaviña, E. Coronado, E. Palomares, *Org. Lett.* **2006**, *8*, 3857–3860; b) E. Coronado, J. R. Galán-Mascarós, C. Martí-Gastaldo, E. Palomares, J. R. Durrant, R. Vilar, M. Gratzel, M. K. Nazeeruddin, *J. Am. Chem. Soc.* **2005**, *127*, 12351–12358; c) A. Caballero, R. Martínez, V. Lloveras, I. Ratera, J. Vidal-Gancedo, K. Wurst, A. Tárrega, P. Molina, J. Veciana, *J. Am. Chem. Soc.* **2005**, *127*, 15666–15667; d) J.-H. Huang, W.-H. Wen, Y.-Y. Sun, P.-T. Chou, J.-M. Fang, *J. Org. Chem.* **2005**, *70*, 5827–5832; e) T. Balaji, M. Sasidharan, H. Matsunaga, *Analyst* **2005**, *130*, 1162–1167.
[8] J. V. Ros-Lis, R. Martínez-Máñez, K. Rurack, F. Sancenón, J. Soto, M. Spieles, *Inorg. Chem.* **2004**, *43*, 5183–5185.
[9] a) A. B. Descalzo, R. Martínez-Máñez, R. Radeglia, K. Rurack, J. Soto, *J. Am. Chem. Soc.* **2003**, *125*, 3418–3419; b) F. Sancenón, R. Martínez-Máñez, J. Soto, *Chem. Commun.* **2001**, 2262–2263; c) K. Rurack, M. Kollmannsberger, U. Resch-Genger, J. Daub, *J. Am. Chem. Soc.* **2000**, *122*, 968–969.
[10] a) S. E. Bailey, T. J. Olin, R. M. Bricka, D. D. Adrian, *Water Res.* **1999**, *33*, 2469–2479; b) A. Dabrowski, Z. Hubicki, P. Podkoscielny, E. Robens, *Chemosphere* **2004**, *56*, 91–106; c) M. Gavrilescu, *Eng. Life Sci.* **2004**, *4*, 219–232.
[11] Most of the sorption materials for $Hg^{2+}$ remediation based on chelating resins and organically modified sol–gel materials are reported

  

to adsorb about 0.05–0.2 g $Hg^{2+}$ per gram of adsorbant. This is in contrast with recently reported organically functionalised mesoporous silica materials, which can adsorb up to 0.3–1.3 g $Hg^{2+}$ per gram of adsorbant.[13,14]

[12] D. A. Atwood, M. K. Zaman, *Struct. Bonding* **2006**, *120*, 163–182.

[13] Recent representative examples: a) C. Sun, R. Qu, C. Ji, Q. Wang, C. Wang, Y. Sun, G. Cheng, *Eur. Polym. J.* **2006**, *42*, 188–194; b) A. Khan, F. Mahmood, Y. Khokhar, S. Ahmed, *React. Funct. Polym.* **2006**, *66*, 1014–1020; c) R. S. Vieira, M. M. Beppu, *Water Res.* **2006**, *40*, 1726–1734; d) G. Wu, Z. Wang, J. Wang, C. He, *Anal. Chim. Acta* **2007**, *582*, 304–310; e) Y.-H. Chang, C.-F. Huang, W.-J. Hsu, F.-C. Chang, *J. Appl. Polym. Sci.* **2007**, *104*, 2896–2905.

[14] a) X. Feng, G. E. Fryxell, L.-Q. Wang, A. Y. Kim, J. Liu, K. M. Kemner, *Science* **1997**, *276*, 923–926; b) J. Liu, X. Feng, G. E. Fryxell, L.-Q. Wang, A. Y. Kim, M. Gong, *Adv. Mater.* **1998**, *10*, 161–165; c) X. Chen, X. Feng, J. Liu, G. E. Fryxell, M. Gong, *Sep. Sci. Technol.* **1999**, *34*, 1121–1132.

[15] L. Mercier, T. J. Pinnavaia, *Adv. Mater.* **1997**, *9*, 500–503.

[16] M. Etienne, S. Sayen, B. Lebeau, A. Walcarius, *Stud. Surf. Sci. Catal.* **2002**, *141*, 615–622.

[17] a) B. Lee, Y. Kim, H. Lee, J. Yi, *Microporous Mesoporous Mater.* **2001**, 50, 77–90; b) R. I. Nooney, M. Kalyanaraman, G. Kennedy, E. J. Maginn, *Langmuir* **2001**, *17*, 528–533; c) V. Antochshuk, M. Jaroniec, *Chem. Commun.* **2002**, 258–259; d) K. A. Venkatesan, T. G. Srinivasan, P. R. V. Rao, *J. Radioanal. Nucl. Chem.* **2003**, *256*, 213–218; e) V. Antochshuk, O. Olkhovyk, M. Jaroniec, I.-S. Park, R. Ryoo, *Langmuir* **2003**, *19*, 3031–3034; f) Y. Kim, B. Lee, J. Yi, *Sep. Sci. Technol.* **2004**, *39*, 1427–1442; g) O. Olkhovyk, M. Jaroniec, *Adsorption* **2005**, *11*, 685–690; h) S. G. Wang, J. L. Li, *Chin. Chem. Lett.* **2006**, *17*, 221–224.

[18] For titania and zirconia analogues, see: R. C. Schroden, M. Al-Daous, S. Sokolov, B. J. Melde, J. C. Lytle, A. Stein, M. C. Carbajo, J. T. Fernández, E. Rodríguez, *J. Mater. Chem.* **2002**, *12*, 3261–3267.

[19] A. B. Descalzo, R. Martínez-Máñez, F. Sancenón, K. Hoffmann, K. Rurack, *Angew. Chem.* **2006**, *118*, 6068–6093; *Angew. Chem. Int. Ed.* **2006**, *45*, 5924–5948.

[20] a) R. Casasús, E. Aznar, M. D. Marcos, R. Martínez-Máñez, F. Sancenón, J. Soto, P. Amorós, *Angew. Chem.* **2006**, *118*, 6813–6816; *Angew. Chem. Int. Ed.* **2006**, *45*, 6661–6664; b) B. García-Acosta, M. Comes, J. L. Bricks, M. A. Kudinova, V. V. Kurdyukov, A. I. Tolmachev, A. B. Descalzo, M. D. Marcos, R. Martínez-Máñez, A. Moreno, F. Sancenón, J. Soto, L. A. Villaescusa, K. Rurack, J. M. Barat, I. Escriche, P. Amorós, *Chem. Commun.* **2006**, 2239–2241; c) M. Comes, M. D. Marcos, R. Martínez-Máñez, M. C. Millan, J. V. Ros-Lis, F. Sancenón, J. Soto, L. A. Villaescusa, *Chem. Eur. J.* **2006**, *12*, 2162–2170; d) M. Comes, G. Rodríguez-López, M. D. Marcos, R. Martínez-Máñez, F. Sancenón, J. Soto, L. A. Villaescusa, P. Amorós, D. Beltrán, *Angew. Chem.* **2005**, *117*, 2978–2982; *Angew. Chem. Int. Ed.* **2005**, *44*, 2918–2922; e) A. B. Descalzo, K. Rurack, H. Weisshoff, R. Martínez-Máñez, M. D. Marcos, P. Amorós, K. Hoffmann, J. Soto, *J. Am. Chem. Soc.* **2005**, *127*, 184–200; f) C. Coll, R. Martínez-Máñez, M. D. Marcos, F. Sancenón, J. Soto, *Angew. Chem.* **2007**, *119*, 1705–1708; *Angew. Chem. Int. Ed.* **2007**, *46*, 1675–1678; g) C. Coll, R. Casasús, E. Aznar, M. D. Marcos, R. Martínez-Máñez, F. Sancenón, J. Soto, P. Amorós, *Chem. Commun.* **2007**, 1957–1959; h) M. Comes, M. D. Marcos, R. Martínez-Máñez, F. Sancenón, J. Soto, L. A. Villaescusa, P. Amorós, D. Beltrán, *Adv. Mater.* **2004**, *16*, 1783–1786.

[21] G. Rodríguez-López, M. D. Marcos, R. Martínez-Máñez, F. Sancenón, J. Soto, L. A. Villaescusa, D. Beltrán, P. Amorós, *Chem. Commun.* **2004**, 2198–2199.

[22] a) K. Rurack, U. Resch-Genger, *Chem. Soc. Rev.* **2002**, *31*, 116–127; b) B. Valeur, I. Leray, *Coord. Chem. Rev.* **2000**, *205*, 3–40; c) A. P. de Silva, H. Q. N. Gunaratne, T. Gunnlaugsson, A. J. M. Huxley, C. P. McCoy, J. T. Rademacher, T. E. Rice, *Chem. Rev.* **1997**, *97*, 1515–1566; d) R. Martínez-Máñez, F. Sancenón, *Chem. Rev.* **2003**, *103*, 4419–4476.

[23] a) S. V. Wegner, A. Okesli, P. Chen, C. He, *J. Am. Chem. Soc.* **2007**, *129*, 3474–3475; b) C.-C. Huang, H.-T. Chang, *Anal. Chem.* **2006**, *78*, 8332–8338; c) Z.-X. Cai, H. Yang, Y. Zhang, X.-P. Yan, *Anal. Chim. Acta* **2006**, *559*, 234–239; d) I.-B. Kim, U. H. F. Bunz, *J. Am. Chem. Soc.* **2006**, *128*, 2818–2819; e) T. J. Dickerson, N. N. Reed, J. J. LaClair, K. D. Janda, *J. Am. Chem. Soc.* **2004**, *126*, 16582–16586; f) A. Ono, H. Togashi, *Angew. Chem.* **2004**, *116*, 4400–4402; *Angew. Chem. Int. Ed.* **2004**, *43*, 4300–4302.

[24] M.-Y. Chae, A. W. Czarnik, *J. Am. Chem. Soc.* **1992**, *114*, 9704–9705.

[25] a) J. V. Ros-Lis, R. Martínez-Máñez, J. Soto, *Chem. Commun.* **2005**, 5260–5262; b) D. Jiménez, R. Martínez-Máñez, F. Sancenón, J. V. Ros-Lis, A. Benito, J. Soto, *J. Am. Chem. Soc.* **2003**, *125*, 9000–9001; c) F. Sancenón, R. Martínez-Máñez, M. A. Miranda, M.-J. Seguí, J. Soto, *Angew. Chem.* **2003**, *115*, 671–674; *Angew. Chem. Int. Ed.* **2003**, *42*, 647–650; d) F. Sancenón, A. B. Descalzo, R. Martínez-Máñez, M. A. Miranda, J. Soto, *Angew. Chem.* **2001**, *113*, 2710–2713; *Angew. Chem. Int. Ed.* **2001**, *40*, 2640–2643; e) J. L. Bricks, K. Rurack, R. Radeglia, G. Reck, B. Schulz, H. Sonnenschein, U. Resch-Genger, *J. Chem. Soc. Perkin Trans. 2* **2000**, 1209–1214.

[26] J. V. Ros-Lis, B. García, D. Jiménez, R. Martínez-Máñez, F. Sancenón, J. Soto, F. Golzalvo, M. C. Valldecabres, *J. Am. Chem. Soc.* **2004**, *126*, 4064–4065.

[27] J. V. Ros-Lis, R. Martínez-Máñez, J. Soto, *Chem. Commun.* **2002**, 2248–2249.

[28] J. V. Ros-Lis, M. D. Marcos, R. Martínez-Máñez, K. Rurack, J. Soto, *Angew. Chem.* **2005**, *117*, 4479–4482; *Angew. Chem. Int. Ed.* **2005**, *44*, 4405–4407.

[29] a) K. C. Song, J. S. Kim, S. M. Park, K.-C. Chung, S. Ahn, S.-K. Chang, *Org. Lett.* **2006**, *8*, 3413–3416; b) Y.-K. Yang, K.-J. Yook, J. Tae, *J. Am. Chem. Soc.* **2005**, *127*, 16760–16761; c) B. Liu, H. Tian, *Chem. Commun.* **2005**, 3156–3158; d) M. Matsushita, M. M. Meijler, P. Wirsching, R. A. Lerner, K. D. Janda, *Org. Lett.* **2005**, *7*, 4943–4946; e) G. Zhang, D. Zhang, S. Yin, X. Yang, Z. Shuai, D. Zhu, *Chem. Commun.* **2005**, 2161–2163; f) G. Hennrich, W. Walther, U. Resch-Genger, H. Sonnenschein, *Inorg. Chem.* **2001**, *40*, 641–644.

[30] S. Cabrera, J. El Haskouri, C. Guillem, J. Latorre, A. Beltrán, D. Beltrán, M. D. Marcos, P. Amorós, *Solid State Sci.* **2000**, *2*, 405–420.

[31] a) P. T. Snee, R. C. Somers, G. Nair, J. P. Zimmer, M. G. Bawendi, D. G. Nocera, *J. Am. Chem. Soc.* **2006**, *128*, 13320–13321; b) V. S. Jisha, K. T. Arun, M. Hariharan, D. Ramaiah, *J. Am. Chem. Soc.* **2006**, *128*, 6024–6025; c) N. Nizomov, Z. F. Ismailov, S. N. Nizamov, M. K. Salakhitdinova, A. L. Tatarets, L. D. Patsenker, G. Khodjayev, *J. Mol. Struct.* **2006**, *788*, 36–42; d) W. Pham, R. Weissleder, C. H. Tung, *Angew. Chem.* **2002**, *114*, 3811–3814; *Angew. Chem. Int. Ed.* **2002**, *41*, 3659–3662; e) E. U. Akkaya, S. Turkyilmaz, *Tetrahedron Lett.* **1997**, *38*, 4513–4516; f) K. G. Thomas, K. J. Thomas, S. Das, M. V. George, *Chem. Commun.* **1997**, 597–598.

[32] a) C. Cornelissen-Gude, W. Rettig, R. Lapouyade, *J. Phys. Chem. A* **1997**, *101*, 9673–9677; b) W. C. Dirk, W. C. Herndon, F. Cervantes-Lee, H. Selnau, S. Martínez, P. Kalamegham, A. Tan, G. Campos, M. Vélez, J. Zyss, I. Ledoux, L. Cheng, *J. Am. Chem. Soc.* **1995**, *117*, 2214–2225; c) P. V. Kamat, S. Das, G. Thomas, M. V. George, *J. Phys. Chem.* **1992**, *96*, 195–199; d) K.-Y. Law, *J. Phys. Chem.* **1987**, *91*, 5184–5193.

[33] See, for instance a) C. T. Kresge, M. E. Leonowicz, W. J. Roth, J. C. Vartuli, J. S. Beck, *Nature* **1992**, *359*, 710–712; b) J. S. Beck, J. C. Vartuli, W. J. Roth, M. E. Leonowicz, C. T. Kresge, K. D. Schmitt, C. T.-W. Chu, D. H. Olson, E. W. Sheppard, S. B. McCullen, J. B. Higgins, J. L. Schlenker, *J. Am. Chem. Soc.* **1992**, *114*, 10834–10843.

[34] a) J. El Haskouri, D. Ortiz de Zárate, C. Guillem, J. Latorre, M. Caldés, A. Beltrán, D. Beltrán, A. B. Descalzo, G. Rodríguez-López, R. Martínez-Máñez, M. D. Marcos, P. Amorós, *Chem. Commun.* **2002**, 330–331; b) L. Huerta, C. Guillem, J. Latorre, A. Beltrán, R. Martínez-Máñez, M. D. Marcos, D. Beltrán, P. Amorós, *Solid State Sci.* **2006**, *8*, 940–951.

[35] a) G. Kickelbick, *Angew. Chem.* **2004**, *116*, 3164–3166; *Angew. Chem. Int. Ed.* **2004**, *43*, 3102–3104; b) A. Stein, *Adv. Mater.* **2003**, *15*, 763–775; c) A. P. Wright, M. E. Davis, *Chem. Rev.* **2002**, *102*, 3589–3614.

[36] **U1** can be readily employed in the pH range 3–9.5.

  

[37] Release of the squaraine dye is not a serious trade-off of the system, since nonhalogenated squaraines do not exhibit high cytotoxicity (cf. D. Ramaiah, I. Eckert, K. T. Arun, L. Weidenfeller, B. Epe, *Photochem. Photobiol.* **2002**, *76*, 672–677; D. Ramaiah, I. Eckert, K. T. Arun, L. Weidenfeller, B. Epe, *Photochem. Photobiol.* **2004**, *79*, 99–104) and simple squaraines such as **III** are photodegraded rather rapidly at elevated temperatures under basic conditions (cf. E. Arunkumar, N. Fu, B. D. Smith, *Chem. Eur. J.* **2006**, *12*, 4684–4690.).
[38] S. Brunauer, P. H. Emmet, E. Teller, *J. Am. Chem. Soc.* **1938**, *60*, 309–319.
[39] E. P. Barret, L. G. Joyner, P. P. Halenda, *J. Am. Chem. Soc.* **1951**, *73*, 373–380.
[40] M. H. Lim, A. Stein, *Chem. Mater.* **1999**, *11*, 3285–3295.
[41] M. Tortajada, D. Ramón, D. Beltrán, P. Amorós, *J. Mater. Chem.* **2005**, *15*, 3859–3868.
[42] a) J. Fan, J. Lei, L. Wang, C. Yu, B. Tu, D. Zhao, *Chem. Commun.* **2003**, 2140–2141; b) J. Lei, J. Fan, C. Yu, L. Zhang, S. Jiang, B. Tu, D. Zhao, *Microporous Mesoporous Mater.* **2004**, *73*, 121–128.
[43] Although the precise determination of the organic content of polyfunctionalised solids such as **U1** can be influenced by incomplete extraction of the surfactant, condensation of an unknown number of silanol groups in thermogravimetric studies or possible condensation of ethanol with silanol groups, the present experiments did not show any peculiarities and, for instance, the thiol contents of UVM-7-SH and **U1** obtained from thermogravimetry and elemental analysis were very similar to the $S/SiO_2$ molar ratio found by energy-dispersive X-ray (EDS) analysis, that is, the data in Table 2 are reliable.
[44] a) G. G. Hoffmann, W. Brockner, I. Steinfatt, *Inorg. Chem.* **2001**, *40*, 977–985; b) P. Biscarini, E. Foresti, G. Pradella, *J. Chem. Soc. Dalton Trans.* **1984**, 953–957.
[45] **G1** also remains completely silent in the presence of the other metal ions and anions tested here.
[46] F. Bernardoni, M. Kouba, A. Y. Fadeev, *Chem. Mater.* **2008**, *20*, 382–387.
[47] As the content of thiol groups is higher in **U1-8** than in **U1**, this material can be loaded with a larger amount of squaraine. However, based on the rationales outlined in the section on optimum loading conditions, **U1-8** contains only approximately twice as many APC groups as **U1**.
[48] A. Bibby, L. Mercier, *Chem. Mater.* **2002**, *14*, 1591–1597.
[49] The drop in the adsorption capability of **U1** suggests that some thiol groups are removed during the first treatment with HCl. Nevertheless, the material still retains a high capacity for $Hg^{2+}$ adsorption and signalling ability. After successive cycles, some mass loss was also observed, most likely due to partial dissolution of the silica support at highly acidic pH.
[50] *Note added in proof*: While this manuscript was in press, another report on a dual-functional hybrid material for $Cu^{2+}$ sensing and adsorption has been published: S. J. Lee, D. R. Bae, W. S. Has, S. S. Lee, J. H. Jung, *Eur. J. Inorg. Chem.* **2008**, 1559–1564.

Received: April 3, 2008
Published online: July 30, 2008

  